Prospects of Holmium-doped fluorides as gain media for visible solid state lasers

F. Reichert,[1,2,*] F. Moglia,[1] P. W. Metz,[1] A. Arcangeli,[3] D.-T. Marzahl,[1] S. Veronesi,[3] D. Parisi,[3] M. Fechner,[1] M. Tonelli,[3] and G. Huber[1,4]

[1]*Institute of Laser-Physics, Luruper Chaussee 149, 22761 Hamburg, Germany*
[2]*Center for Free-Electron Laser Science, DESY, Notkestrasse 85, 22607 Hamburg, Germany*
[3]*NEST-Istituto Nanoscienze-CNR and Dipartimento di Fisica, Università di Pisa, B. Pontecorvo 3, 56127 Pisa, Italy*
[4]*The Hamburg Centre for Ultrafast Imaging, Luruper Chaussee 149, 22761 Hamburg, Germany*
**Fabian.Reichert@desy.de*

Abstract: In this paper we report on the suitability of Ho^{3+}:$LiLuF_4$ and Ho^{3+}:LaF_3 as active media for solid state lasers emitting in the green spectral region. The ground state absorption spectra were measured and employed to calculate the emission cross section spectra via the reciprocity method. These allowed to derive the gain characteristics for various inversion ratios. The decay dynamics of the $^5F_4$,$^5S_2$ multiplet, which would act as upper laser level, were investigated to estimate the quantum efficiency. Measurements of the excited state absorption were conducted which showed that stimulated emission is the dominating effect around 550 nm. Laser operation was demonstrated in the green spectral region by employing Ho^{3+}:LaF_3 as gain medium. Laser oscillation occurred in a self-pulsed regime with a maximum average output power of 7.7 mW, a repetition rate of 5.3 kHz, and a pulse duration of 1.6 µs. To the best of our knowledge this constitutes the first green laser emission of a Ho^{3+}-doped crystal at room temperature.

OCIS codes: (140.3380) Laser materials; (140.7300) Visible lasers; (300.6550) Spectroscopy, visible.

References and links

1. T. Gün, P. Metz, and G. Huber, "Power scaling of laser diode pumped Pr^{3+}:$LiYF_4$ cw lasers: efficient laser operation at 522.6 nm, 545.9 nm, 607.2 nm, and 639.5 nm," Opt. Lett. **36**, 1002–1004 (2011).
2. F. Reichert, D.-T. Marzahl, P. Metz, M. Fechner, N.-O. Hansen, and G. Huber, "Efficient laser operation of Pr^{3+},Mg^{2+}:$SrAl_{12}O_{19}$," Opt. Lett. **37**, 4889–4891 (2012).
3. M. Fibrich, H. Jelínková, J. Šulc, K. Nejezchleb, and V. Škoda, "Visible cw laser emission of GaN-diode pumped Pr:$YAlO_3$ crystal," Appl. Phys. B **97**, 363–367 (2009).
4. F. Reichert, T. Calmano, S. Müller, D.-T. Marzahl, P. W. Metz, and G. Huber, "Efficient visible laser operation of Pr,Mg:$SrAl_{12}O_{19}$ channel waveguides," Opt. Lett. **38**, 2698–2701 (2013).
5. Andreas Voss, Fabian Reichert, Philip Werner Metz, Daniel-Timo Marzahl, Christian Kränkel, Günter Huber, and Thomas Graf, "Thin-disk laser operation of Pr^{3+},Mg^{2+}:$SrAl_{12}O_{19}$," Opt. Lett. **39**, 1322–1325 (2014)
6. T. Danger, J. Koetke, R. Brede, E. Heumann, G. Huber, and B. H. T. Chai, "Spectroscopy and green upconversion laser emission of Er^{3+}-doped crystals at room temperature," J. Appl. Phys. **76**, 1413–1422 (1994).
7. F. Moglia, S. Müller, T. Calmano, and G. Huber, "Er:$LiLuF_4$ upconversion waveguide laser fabricated by femtosecond-laser writing," 5th EPS-QEOD EUROPHOTON Conference 2012, Stockholm, Sweden, paper TuB.25 (2012).

#222481 - $15.00 USD Received 4 Sep 2014; revised 10 Nov 2014; accepted 10 Nov 2014; published 10 Dec 2014

8. B. P. Scott, F. Zhao, R. S. F. Chang, and N. Djeu, “Upconversion-pumped blue laser in Tm:YAG," Opt. Lett. **18**, 113–115 (1993).
9. S. R. Bowman, S. O’Connor, and N. J. Condon, “Diode pumped yellow dysprosium lasers," Opt. Express **20**, 12906–12911 (2012).
10. P. W. Metz, F. Moglia, F. Reichert, S. Müller, D.-T. Marzahl, N.-O. Hansen, C. Kränkel, and G. Huber, “Novel Rare Earth Solid State Lasers with Emission Wavelengths in the Visible Spectral Range," Conference on Lasers and Electro-Optics (CLEO/Europe - EQEC) 2013, Munich, Germany, paper: CA-2.5, (2013).
11. B. N. Kazakov, M. S. Orlov, M. V. Petrov, A. L. Stolov, and A.M. Tkachuk, “Induced emission of Sm^{3+} ions in the visible region of the spectrum," Optics and Spectroscopy **47**, 676 (1979).
12. H. Jenssen, D. Castleberry, D. Gabbe, and A. Linz, “Stimulated emission at 5445 Å in Tb^{3+}:YLF," IEEE J. Quantum Elec. **9**, 665 (1973).
13. Y. K. Voron’ko, A. A. Kaminski, and V. V. Osiko, and A. M. Prokhorov, “Stimulated Emission of Ho^{3+} in CaF_2 at $\lambda = 5512$ Å," JETP Lett. **1**, 3 (1965).
14. L. F. Johnson and H. J. Guggenheim, “Infrared-Pumped Visible Laser," Appl. Phys. Lett. **19**, 44–47 (1971).
15. E. Chicklis, C. Naiman, L. Esterowitz, and R. Allen, “Deep red laser emission in Ho:YLF," IEEE J. Quantum Elec. **13**, 893–895 (1977).
16. J. Y. Allain, M. Monerie, and H. Poignant, “Room temperature CW tunable green upconversion holmium fibre laser," Electron. Lett. **26**, 261–263 (1990).
17. David S. Funk and J. G. Eden, “Laser diode-pumped holmium-doped fluorozirconate glass fiber laser in the green ($\lambda \sim$544-549 nm): power conversion efficiency, pump acceptance bandwidth, and excited-state kinetics," IEEE J. Quantum Elec. **37** 980–992 (2001).
18. Brian M. Walsh, Gary W. Grew, and Norman P. Barnes, “Energy levels and intensity parameters of Ho^{3+} ions in $LiGdF_4$,$LiYF_4$, and $LiLuF_4$," J. Phys. - Condens. Mat. **17**, 7643–7665 (2005).
19. H. Scheife, G. Huber, E. Heumann, S. Bär, and E. Osiac, “Advances in up-conversion lasers based on Er^{3+} and Pr^{3+}," Opt. Mater. **26**, 365–374 (2004).
20. W. M. Yen, W. C. Scott, and A. L. Schawlow, “Phonon-Induced Relaxation in Excited Optical States of Trivalent Praseodymium in LaF_3," Phys. Rev. **136**, A271–A283 (1964).
21. S. Nakamura, M. Senoh, S. Nagahama, N. Iwasa, T. Yamada, T. Matsushita, H. Kiyoku, and Y. Sugimoto, “InGaN-Based Multi-Quantum-Well-Structure Laser Diodes," Jpn. J. Appl. Phys. **35**, L74 (1996).
22. J. L. A. Chilla, S. D. Butterworth, A. Zeitschel, J. P. Charles, A. L. Caprara, M. K. Reed, and L. Spinelli, “High-power optically pumped semiconductor lasers," Proc. SPIE **5332**, Solid State Lasers XIII: Technology and Devices, 143 (2004).
23. Francesco Cornacchia, Daniela Parisi, and Mauro Tonelli, “Spectroscopy and Diode-Pumped Laser Experiments of $LiLuF_4$:Tm^{3+} Crystals," IEEE J. Quant. Elec. **44**, 1076–1082 (2008).
24. F. Reichert and F. Moglia and D. T. Marzahl and P. Metz and M. Fechner and N.-O. Hansen, and G. Huber, “Diode pumped laser operation and spectroscopy of Pr^{3+}:LaF_3," Opt. Express **20**, 20387–20395 (2012).
25. Brian M. Walsh, Norman P. Barnes, and Baldassare Di Bartolo, “Branching ratios, cross sections, and radiative lifetimes of rare earth ions in solids: Application to Tm^{3+} and Ho^{3+} ions in $LiYF_4$," J. Appl. Phys. **83**, 2772–2787 (1998).
26. D. E. McCumber, “Einstein Relations Connecting Broadband Emission and Absorption Spectra," Phys. Rev. **136**, A954–A957 (1964).
27. H. H. Caspers, H. E. Rast, and J. L. Fry, “Absorption, Fluorescence, and Energy Levels of Ho^{3+} in LaF_3," J. Chem. Phys. **53**, 3208–3216 (1970).
28. J. B. Gruber, M. E. Hills, M. D. Seltzer, S. B. Stevens, C. A. Morrison, G. A. Turner, and M. R. Kokta, “Energy levels and crystal quantum states of trivalent holmium in yttrium aluminum garnet," J. Appl. Phys. **69**, 8183–8204 (1991).
29. Philipp Koopmann, “Thulium- and Holmium-doped Sesquioxides for 2 µm Lasers ," Ph.D.-thesis, University of Hamburg (2012).
30. L. A. Riseberg and H. W. Moos, “Multiphonon Orbit-Lattice Relaxation of Excited States of Rare-Earth Ions in Crystals," Phys. Rev. **174**, 429–438 (1968).
31. X. X. Zhang, A. Schulte, and B. Chai, “Raman spectroscopic evidence for isomorphous structure of $LiGdF_4$ and $LiYF_4$ laser crystals," Solid State Commun. **89**, 181 (1994).
32. L. Gomes, L. C. Courrol, L. V. G. Tarelho, and I. M. Ranieri, “Cross-relaxation process between +3 rare-earth ions in $LiYF_4$ crystals," Phys. Rev. B **54**, 3825–3829 (1996).
33. G. K. Liu, Y. H. Chen, and J. V. Beitz, “Photon avalanche up-conversion in Ho^{3+} doped fluoride glasses," J. Lumin. **81**, 7–12 (1999).
34. J. A. Capobianco, J. C. Boyer, F. Vetrone, A. Speghini, and M. Bettinelli, “Optical Spectroscopy and Upconversion Studies of Ho^{3+}-Doped Bulk and Nanocrystalline Y_2O_3," Chem. Mat. **14**, 2914–2921 (2002).
35. M. Malinowski, M. Kaczkan, A. Wnuk, and M. Szufliñska, “Emission from the high lying excited states of Ho^{3+} ions in YAP and YAG crystals," J. Lumin. **106**, 269–279 (2004).
36. J. Koetke and G. Huber, “Infrared excited-state absorption and stimulated-emission cross sections of Er^{3+}-doped crystals," Appl. Phys. B **61**, 151–158 (1995).

#222481 - $15.00 USD Received 4 Sep 2014; revised 10 Nov 2014; accepted 10 Nov 2014; published 10 Dec 2014

1. Introduction

In recent time substantial attention was given to the development of novel gain media for solid state lasers emitting in the visible spectral region. Work was mainly focused on Pr^{3+}-doped crystals where efficient laser operation was demonstrated with a variety of host materials and resonator geometries [1–5]. But also other elements of the rare-earth series have been shown to enable laser operation in the visible spectral region. Interesting results have been obtained for example with Er^{3+} [6, 7], Tm^{3+} [8], Dy^{3+} [9, 10], Sm^{3+} [10, 11], and Tb^{3+} [10, 12] and so it seems worthwhile to investigate further possibilities. In general, lasers operating in the visible spectral region are interesting for a broad range of applications. They can be employed as light sources for display and entertainment technology, to excite dyes in fluorescence microscopes, for quantum optical experiments, as well as for optical storage schemes.

First reports of employing Ho^{3+}-doped crystals as gain media for visible lasers were made by Voron'ko *et al.* and Johnson *et al.* [13, 14]. Both demonstrated laser oscillation in the green spectral range on the transition $^5F_4,^5S_2 \rightarrow ^5I_8$ (cf. Fig. 1) at cryogenic temperatures under Xe-flash-lamp pumping. At room temperature, visible laser operation has so far only been demonstrated on the transition $^5F_4,^5S_2 \rightarrow ^5I_7$ in the deep red spectral region with the first results being reported by Chicklis et al. [15]. Green laser emission of Ho^{3+}-doped gain media at room temperature was so far only achieved in Ho^{3+}-doped ZBLAN fibers [16, 17].

The relatively small number of visible lasers realized with Ho^{3+}-doped gain media might stem from a property of the energy level scheme (cf. Fig. 1 and [18]): the distance between the upper laser level $^5F_4,^5S_2$ and the next lower level $^5F_5$ is roughly 2900 cm^{-1}. If the phonon energy of the host system is too high it will facilitate a strong multi-phonon relaxation and thus a low quantum efficiency of the $^5F_4,^5S_2$ multiplet. In addition, a laser based on the transition $^5F_4,^5S_2 \rightarrow ^5I_8$ is of the quasi-three-level nature and therefore reabsorption must be bleached before gain can be achieved. Depending on the Stark splitting of the involved multiplets, which is also strongly dependent on the host matrix, this can mean that high inversion rates must be realized before laser oscillation can take place. The combination of these two features of the trivalent holmium ion necessitates that great care must be taken in choosing the host matrix.

In this paper two Ho^{3+}-doped fluoride crystals, Ho^{3+}:$LiLuF_4$ (Ho:LLF) and Ho^{3+}:LaF_3 were

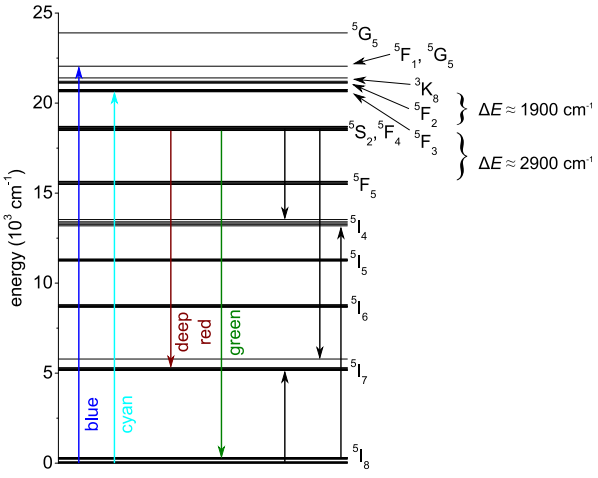

Fig. 1: Schematic energy level diagram of Ho^{3+} based on [18]. Colored arrows indicate photon-assisted transitions while black arrows show possible cross relaxation processes.

#222481 - $15.00 USD Received 4 Sep 2014; revised 10 Nov 2014; accepted 10 Nov 2014; published 10 Dec 2014

investigated for their suitability as gain medium for solid state lasers in the visible spectral region. Both host systems were chosen due to their low phonon energies of <430 cm^{-1} [19] and 340 cm^{-1} [20] respectively. Crystalline samples were fabricated and analyzed for various spectroscopic properties. Ground state absorption (GSA) spectra were recorded to investigate the possibility of direct pumping via blue laser sources which have been developed in recent years [21,22]. The GSA characteristics have also been used to derive the emission cross sections via the reciprocity method. In the case of Ho:LaF_3 it was also necessary to conduct transmission measurements at cryogenic temperatures to determine the energy level positions of the five Stark levels composing the $^5S_2$ multiplet. The decay dynamics of the upper laser level were recorded in the temperature range between 10 K and 300 K, which allowed to estimate the quantum efficiency. Measurements of the excited state absorption (ESA) were conducted to investigate, whether or not absorption into higher energy levels is present. Finally, laser experiments were carried out, which, to the best of our knowledge, yielded the first green emitting laser based on a crystalline Ho^{3+}-doped gain medium at room temperature.

2. Spectroscopy

In order to evaluate the suitability of both systems various spectroscopic properties were investigated. Single crystalline samples were fabricated by the standard Czochralski technique for Ho:LLF, and by slowly cooling down the melt in case of Ho:LaF_3. More information on the setups and growth parameters can be found in [23] and [24] respectively.

2.1. Ground state absorption at room temperature

The polarization dependent ground state absorption spectra of Ho:LaF_3 and Ho:LLF were recorded with a *Varian* Cary 5000 UV-Vis-NIR. Measurements were carried out with *a*-cut samples with thicknesses of 3.1 mm (Ho:LLF) and 3.0 mm (Ho:LaF_3). The dopant concentrations of the samples were 0.6 at.% and 0.4 at.%, respectively, which was determined by microprobing. The resolution was chosen in accordance to the minimum linewidths of the spectra and was set to 0.3 nm for both systems. GSA cross sections were derived by employing the Lambert-Beer law. Two different wavelength ranges were investigated. The blue spectral region, between 430 nm and 495 nm, is interesting for pumping, while the absorption cross sections in the green spectral range, between 515 nm and 555 nm, are necessary to determine the emission cross sections and gain spectra at the prospective laser wavelengths. The recorded spectra are depicted in Fig. 2 with a summary of the characteristics of the most prominent peaks in Tab. 1.

Maxima in the ground state absorption spectra of Ho:LLF can be found at wavelengths of 452.9 nm (π), 486.0 nm (π), and 535.2 nm (π) with absorption cross sections of $3.8 \cdot 10^{-20}$ cm^2, $2.0 \cdot 10^{-20}$ cm^2, and $8.3 \cdot 10^{-20}$ cm^2 respectively. The first peak which corresponds to the $^5I_8 \rightarrow {}^5F_1$, $^5G_6$ transition can be addressed with InGaN LDs although its narrow linewidth ($\Delta\lambda \approx 0.6$ nm) may lead to a poor overlap between pump and absorption spectra. The overlap could be improved by employing for example grating stabilized LDs. The second peak which corresponds to the $^5I_8 \rightarrow {}^5F_3$ transition allows for pumping with 2ωOPSLs. Here the narrow linewidth of the absorption peak is not problematic since the emission spectrum of 2ωOPSLs is narrow ($\Delta\lambda < 0.1$ nm) and thus ensures a good spectral overlap. In general it can be said that the shape of the obtained spectra and the values of the absorption cross sections in the green spectral region are in good agreement with the spectra reported by Walsh *et al.* for the isomorphic system Ho^{3+}:$LiYF_4$ [25].

In the case of Ho:LaF_3, highest absorption cross sections can be found at wavelengths of 447.3 nm (σ), 482.7 nm (π), and 533.8 nm (π) with values of $1.4 \cdot 10^{-20}$ cm^2, $0.3 \cdot 10^{-20}$ cm^2, and $0.8 \cdot 10^{-20}$ cm^2. Although the GSA cross sections in Ho:LaF_3 are generally smaller than in Ho:LLF, the linewidths are in turn larger, which should allow for a more efficient absorption

#222481 - $15.00 USD Received 4 Sep 2014; revised 10 Nov 2014; accepted 10 Nov 2014; published 10 Dec 2014

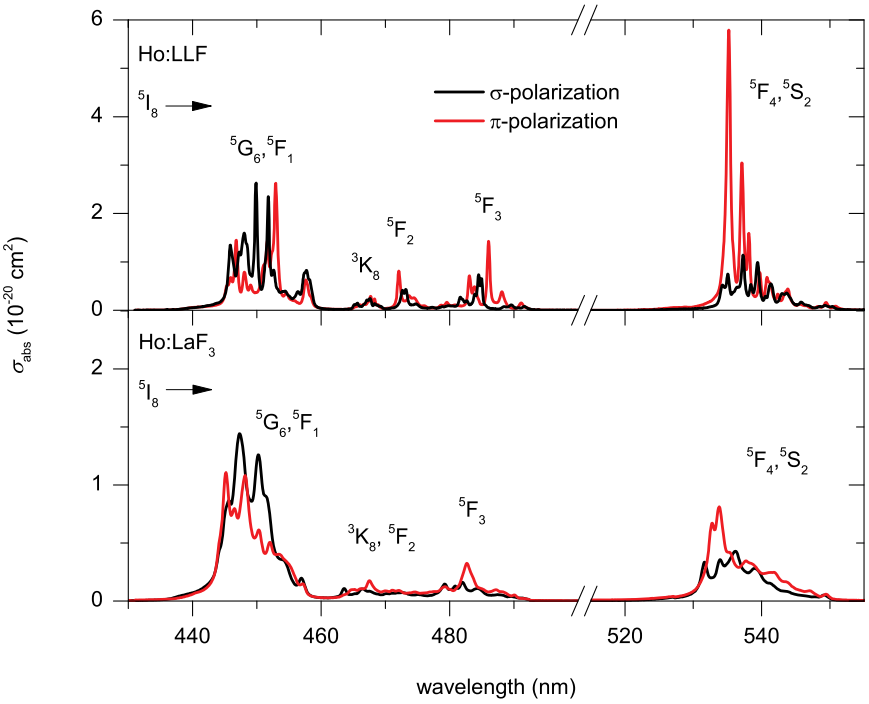

Fig. 2: Polarization dependent ground state absorption spectra derived for Ho:LLF (upper) and Ho:LaF_3 (lower).

of pump light delivered by InGaN LDs. An interesting feature is the substantial absorption at 532.0 nm ($\sigma_{abs} = 3.3 \cdot 10^{-21}$ cm^2). This may give rise to the possibility of an in-band pumping scheme by employing high power frequency doubled Nd^{3+} lasers or, in the future, green emitting laser diodes. Such a pumping scheme would have the advantage of a very small quantum defect of less than 3 % which leads to a very small thermal load of the crystal.

2.2. Ground state absorption at cryogenic temperature

Since not all energetic positions of the five Stark levels of the $^5S_2$ multiplet in Ho:LaF_3 have been reported so far, transmission measurements were conducted at a temperature of 10 K. Here, a spectrally broad emitting halogen lamp was imaged onto a variable aperture with an optical chopper placed behind it. It was then imaged with a second lens onto a 2 mm thick 0.3 at.% doped sample, which was placed on a 2 mm aperture inside a *Leybold* ROK 10/300 cryostat. The variable aperture allowed for adjusting the spot size on the sample and thus to prevent a heating of the sample holder and the sample itself. A third lens imaged the transmitted light onto the entrance slit of a *SPEX 1000* monochromator. A Si-diode placed at the exit slit of the monochromator detected the light and in combination with a *Stanford Research Inc.* SR 810 DSP lock-in amplifier which was supplied with the reference signal of the chopper this setup allowed for an excellent signal-to-noise ratio. The resolution of the monochromator was set to 40 pm.

At 10 K only the lowest Stark level of the $^5I_8$ multiplet is populated. The recorded transmission spectrum shows five absorption bands with Gaussian line shapes. These bands correspond to the transitions into the five Stark levels of the $^5S_2$ manifold. Gaussian fits revealed the energetic position of each level. The results are listed in Tab. 2.

#222481 - $15.00 USD Received 4 Sep 2014; revised 10 Nov 2014; accepted 10 Nov 2014; published 10 Dec 2014

Table 1: Peak absorption wavelengths λ_{GSA} and cross sections σ_{GSA} of the Ho^{3+}-doped systems with corresponding polarization and transition assignment. Linewidths $\Delta\lambda$ (FWHM) given in parentheses indicate a structure of the corresponding absorption peak and values are given for the whole band.

system	λ_{GSA} (nm)	σ_{GSA} (10^{-20} cm^2)	$\Delta\lambda$ (nm)	polarization	transition
Ho:LLF	449.9	3.6	0.6	σ	$^5I_8 \rightarrow {}^5F_1, {}^5G_6$
	452.9	3.8	0.9	π	
	484.5	1.1	1.0	σ	$^5I_8 \rightarrow {}^5F_3$
	486.0	2.0	0.6	π	
	537.3	1.6	0.9	σ	$^5I_8 \rightarrow {}^5F_4, {}^5S_2$
	535.2	8.3	0.7	π	
Ho:LaF_3	447.3	1.4	(7.2)	σ	$^5I_8 \rightarrow {}^5F_1, {}^5G_6$
	445.2	1.1	(6.4)	π	
	482.7	0.3	2.2	π	$^5I_8 \rightarrow {}^5F_3$
	536.2	0.4	-	σ	$^5I_8 \rightarrow {}^5F_4, {}^5S_2$
	533.8	0.8	(3.3)	π	

2.3. Emission

The obtained ground state absorption cross sections were used to derive the emission cross sections of the $^5F_4, {}^5S_2 \rightarrow {}^5I_8$ transition via the reciprocity method [26]. For Ho:LLF the necessary energetic positions of the involved manifolds were taken as reported by Walsh *et al.* [25]. In the case of Ho:LaF_3, Caspers *et al.* reported the data for the multiplets $^5I_8$ and $^5F_4$ [27]. The position of the five Stark levels composing the $^5S_2$ manifold were taken from the preceding section.

The emission cross sections derived for Ho:LLF are depicted in Fig. 3a and the most important values are listed in Tab. 3. It can be seen that the emission band corresponding to the $^5F_4, {}^5S_2 \rightarrow {}^5I_8$ transition consists of several narrow linewidth peaks. The maximum emission cross section of $19.1 \cdot 10^{-21}$ cm^2 can be found in the spectrum for π-polarized light at a wavelength of 535.3 nm. The maxima at 549.5 nm and 550.9 nm with emission cross sections of $5.4 \cdot 10^{-21}$ cm^2 and $3.6 \cdot 10^{-21}$ cm^2, respectively, are of special interest since they are less affected by reabsorption. The increasing noise level towards the longer wavelength part of the spectrum is an artifact produced by the reciprocity method. It results from a factor in the reciprocity equation which grows exponential for wavelengths further away from the zero-phonon

Table 2: Energetic positions of the five Stark levels composing the $^5S_2$ manifold in Ho:LaF_3.

	No.	energy (cm^{-1})	wavelength (nm)
$^5S_2$	1	18600	537.65
	2	18605	537.49
	3	18609	537.37
	4	18621	537.03
	5	18625	536.91

#222481 - $15.00 USD Received 4 Sep 2014; revised 10 Nov 2014; accepted 10 Nov 2014; published 10 Dec 2014

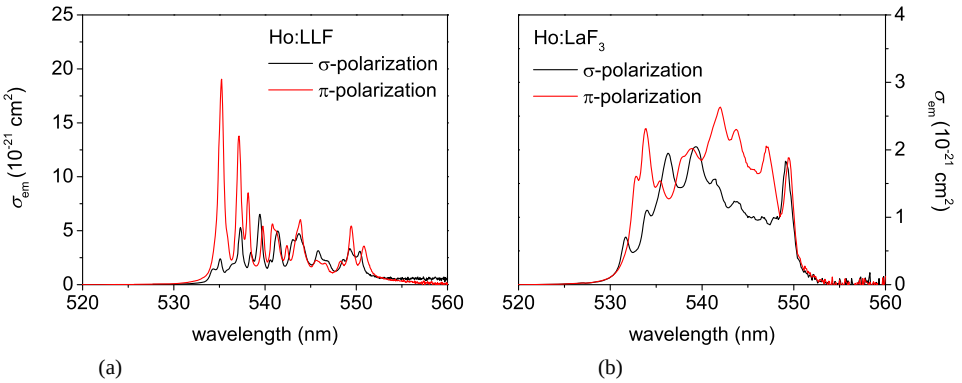

Fig. 3: Polarization dependent emission spectra of the $^5F_4,^5S_2 \rightarrow ^5I_8$ transition in Ho:LLF (a) and Ho:LaF_3 (b).

line and thus magnifies the trailing noise. As it was the case for the absorption characteristics, the shape of the spectrum as well as the values of the emission cross sections are in good agreement with those reported by Walsh *et al.* for the isomorphic system Ho^{3+}:$LiYF_4$ [25].

The emission spectra derived for Ho:LaF_3 are depicted in Fig. 3b. In contrast to Ho:LLF the emission peaks exhibit larger linewidths but in turn smaller peak emission cross sections. The maximum value of $2.6 \cdot 10^{-21}$ cm^2 can be found at a wavelength of 542.0 nm (π). At the long wavelength edge of the emission band a peak with an emission cross section of $1.9 \cdot 10^{-21}$ cm^2 can be found at 549.4 nm.

2.4. Gain

From the GSA and emission characteristics the gain cross sections were derived via the relation $\sigma_{\text{gain}} = \beta\ \sigma_{\text{em}} - (1-\beta)\sigma_{\text{abs}}$. Here, β is the inversion rate and follows from the population density of the upper laser level N_2 and the total density of Ho^{3+}-ions N_{tot} via $\beta = \frac{N_2}{N_{\text{tot}}}$.

The polarization dependent gain spectra of Ho:LLF for various values of β are depicted in Fig. 4a and Fig. 4b. It can be seen that independent of the polarization more than 20 % of the active ions have to be excited into the upper laser level to saturate the reabsorption and to achieve gain. Above this level two peaks with positive gain emerge at wavelengths of

Table 3: Peak emission wavelengths λ_{em} and cross sections σ_{em} of Ho^{3+}-doped media with corresponding polarization and transition assignment.

system	λ_{em} (nm)	σ_{em} (10^{-21} cm^2)	$\Delta\lambda$ (nm)	polarization	transition
Ho:LLF	532.3	19.1	0.6	π	$^5F_4,^5S_2 \rightarrow ^5I_8$
	549.5	5.4	1.0	π	
	550.8	3.6	0.9	π	
Ho:LaF_3	533.9	2.3	-	π	$^5F_4,^5S_2 \rightarrow ^5I_8$
	542.0	2.6	-	π	
	549.4	1.9	-	π	
	549.1	1.8	-	σ	

#222481 - $15.00 USD Received 4 Sep 2014; revised 10 Nov 2014; accepted 10 Nov 2014; published 10 Dec 2014

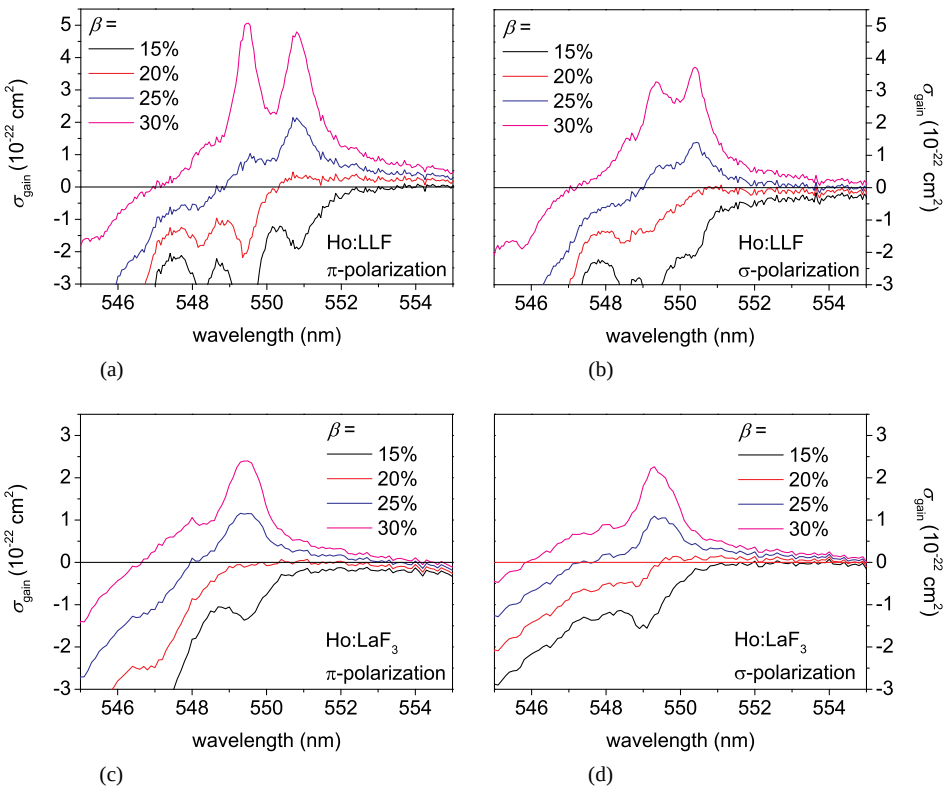

Fig. 4: Polarization dependent gain spectra of the $^5F_4$,$^5S_2 \rightarrow {}^5I_8$ transition in Ho:LLF (a,b) and Ho:LaF_3 (c,d).

549.5 nm and 550.8 nm. For π-polarized light and inversion levels between 20 % - 30 % the long wavelength peak is dominant while above roughly 30 % the short wavelength peak exhibits a higher gain.

As it can be seen in Fig. 4c and Fig. 4d, the situation is quite similar for Ho:LaF_3. Again an inversion level of more than 20 % is necessary to achieve gain independent of the polarization. At higher β-levels a single peak emerges at a wavelength of 549.4 nm.

The high inversion densities necessary to bleach the reabsorption in Ho^{3+}-doped fluoride materials can be attributed to a strong overlap of the absorption and emission bands. This is due to the relatively weak Stark splitting, especially of the $^5I_8$ ground state which causes a non-negligible Boltzman population even for higher lying Stark levels. The high number of levels composing the ground state therefore present numerous starting points for possible absorption transitions. However, host systems where the involved levels exhibit a stronger splitting, e.g. Ho^{3+}:$Y_3Al_5O_{12}$ [28] or Ho^{3+}:Sc_2O_3 [29] have higher phonon energies and therefore less favorable non-radiative decay rates of the $^5F_4$,$^5S_2$ multiplet.

2.5. Fluorescence decay dynamics

In order to evaluate the non-radiative coupling between the multiplets $^5F_4$,$^5S_2$ and $^5F_5$ and subsequently the quantum efficiency of the upper laser level, the decay dynamics of the former multiplet were investigated at temperatures between 10 K and 300 K. For this, samples of Ho:LLF and Ho:LaF_3 were excited by an OPO driven by the third harmonic of a Nd:YAG laser

#222481 - $15.00 USD Received 4 Sep 2014; revised 10 Nov 2014; accepted 10 Nov 2014; published 10 Dec 2014

operating at $\lambda = 1064\,\text{nm}$. It operated with a repetition rate of 10 Hz and with a pulse duration of 20 ns. The fluorescence light was collimated and focused by a pair of lenses onto the entrance slit of a *SPEX 500* monochromator to enable a spectral selection of the light originating from the transition $^5F_4,^5S_2 \rightarrow {}^5I_8$. The signal was detected by a *Hamamatsu* S1 PMT and fed into an oscilloscope, which averaged the temporal evolution of the fluorescence over 500 pulses to reduce the noise level. The samples were placed in a *Leybold* ROK 10/300 cryostat, which allowed to choose temperatures between 10 K and 300 K. To suppress reabsorption and cross relaxation effects, low doped (0.3 at.%) samples and small excitation volumes were chosen.

To measure the decay dynamics in Ho:LLF, an excitation wavelength of $\lambda_{ex} = 537\,\text{nm}$ was chosen while the signal was detected at $\lambda_{em} = 549\,\text{nm}$. The recorded decay curves are depicted in a semi-logarithmic plot in Fig. 5a. It can be seen that all curves exhibit a single exponential decay, which indicates that no interionic interactions are present that might distort the measurement. Effective lifetimes τ_{eff} were derived via two different ways, by integrating over the whole curve and by single exponential fits. The difference between the two methods is less than 5 % with the following values resulting from the latter method. As it can be seen in Fig. 5a τ_{eff} increases from 99 µs at 300 K to 234 µs at 50 K which could be caused either by lower multiphonon relaxation rates due to the freezing out of phonons, or by higher transition probabilities for the higher lying $^5F_4$ multiplet which is depopulated towards lower temperatures. However, the progression of τ_{eff} and the population of the $^5F_4$ multiplet with temperature exhibit a different fashion and it is therefore assumed that the decrease of the lifetimes is cause by smaller mulitphonon relaxation rates. This means that at room temperature a substantial amount of excited ions decay non-radiatively. For 10 K τ_{eff} decreases to 227 µs.

To estimate the quantum efficiency η_q the multi-phonon relaxation W_{mp} at $T = 10\,\text{K}$ was approximated to be zero which means that the effective lifetime measured at this temperature can be taken as the radiative lifetime τ_{rad}. Assuming furthermore that no other processes quench the lifetime at room temperature, W_{mp} can then be derived via the relation $W_{mp} = \frac{1}{\tau_{rad}} - \frac{1}{\tau_{eff}}$. The quantum efficiency then follows from $\eta_q = 1 - W_{mp} \cdot \tau_{eff}$. It should be noted though that this is an upper limit for η_q since even at 10 K a residual multi-phonon decay might be present [30]. For Ho:LLF this leads to a quantum efficiency of roughly 40 %. This means that despite the low phonon energy of the $LiLuF_4$ matrix [31] an efficient coupling of the upper laser level and the next lower level is present and that more than half of the excited ions decay via a multi-phonon relaxation.

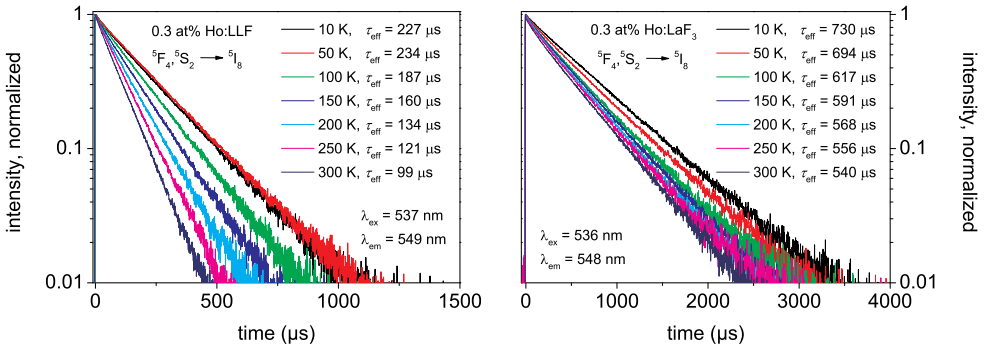

(a) (b)

Fig. 5: Temperature dependent decay dynamics of the $^5F_3$ and $^5F_4,^5S_2$ multiplets in Ho:LLF (a) and Ho:LaF_3 (b). Values of τ_{eff} were derived via single exponential fits.

#222481 - $15.00 USD Received 4 Sep 2014; revised 10 Nov 2014; accepted 10 Nov 2014; published 10 Dec 2014

In the case of Ho:LaF_3 the excitation wavelength was chosen to be $\lambda_{ex} = 536$ nm while the monochromator was set for $\lambda_{em} = 548$ nm. As it can be seen from Fig. 5b the evolution of the fluorescence signal in the first few hundred microseconds does not exhibit a single exponential behavior. It is thus well possible that cross relaxation processes take place [32–35]. This also leads to a deviation between the effective lifetimes obtained by fitting in the interval where the decay is single exponential and by integrating over the whole curve. The difference increases from a low value of 4 % at 10 K to substantial 14 % at 300 K. This indicates that at low temperatures the impact of the cross relaxation process is small, which is most likely due to a decreased spectral overlap between the involved transitions. It can also be seen that the decrease of τ_{eff} itself is less severe towards higher temperatures than in Ho:LLF. The effective lifetime shortens from $\tau_{eff} = 730$ µs at 10 K to $\tau_{eff} = 540$ µs at 300 K. Values were taken from the fits in order to compensate for the shortening due to the cross relaxation process. Assuming 730 µs as the radiative lifetime, at room temperature a minimum of 25 % of the excited ions decay via multi-phonon relaxation which is substantially less than in the case of Ho:LLF.

2.6. Excited state absorption

The high number of multiplets present in Ho^{3+} leads to the possibility of detrimental ESA into higher lying energy levels. To investigate whether or not this effect occurs, measurements based on the setup proposed in [36] were carried out. The probe beam was delivered by a 450 W Xe lamp. As pump sources a frequency doubled Nd^{3+}:YVO_4 laser with $\lambda_{em} = 532$ nm as well as InGaN LDs with a central emission wavelength in the 450 nm range fitting to the absorption peak of the respective material were employed. The reason for using various pump sources was that due to the setup, scattered pump light leads to artifacts in the direct spectral vicinity of the central emission wavelength of the pump. In order to obtain a complete spectrum, measurements were carried out by either pumping in the green or in the blue spectral region, normalizing the recorded spectra to each other, and, finally, combining them. For Ho:LLF measurements were also carried out by employing a Tm^{3+}:Lu_2O_3 laser emitting at 2065 nm. This was done since it is likely that due to the pronounced multi-phonon relaxation of the $^5F_4$,$^5S_2$ multiplet and the relatively long lifetime of the $^5I_7$ multiplet ($\tau_{rad} = 14$ ms [18]) a considerable amount of population is trapped in the latter manifold and it can thus act as starting level for ESA. The resolution was set to 0.8 nm which was necessary due to the generally low signal that is inherent to this type of measurement.

It follows from [36] that the obtained spectra are superpositions of $\sigma_{GSA,i}(\lambda)$, $\sigma_{em,i}(\lambda)$ and $\sigma_{ESA,i}(\lambda)$ of the i populated levels. They can be calibrated with the priorly derived GSA cross sections at a point in the spectrum which only exhibits GSA bleaching. Subsequent subtraction of the GSA characteristics leaves spectra composed of ESA and stimulated emission. Doing this for Ho:LLF leads to the spectra depicted in Fig. 6 where the upper part results from pumping in the visible spectral range ($\lambda_{ex} = 449$ nm/532 nm) and the lower part from pumping in the NIR ($\lambda_{ex} = 2065$ nm). In these graphs stimulated emission is denoted with a positive sign while ESA carries a negative sign. It can be seen that most ESA bands are present for pumping in the visible as well as in the near infrared spectral region. This leads to the conclusion that these bands do not result from ESA transitions starting from the upper laser level $^5F_4$,$^5S_2$ but from the trapping multiplet $^5I_7$. The comparison of the photon energies of these ESA processes with the energy level diagram in Fig. 1 shows that the transitions marked as 1 - 6 in Fig. 6 fit to the energetic distances between the multiplet $^5I_7$ and various higher Stark multiplets (cf. Tab. 4). The most pronounced difference between the upper and the lower spectra can be found around 550 nm marked as A. In the upper spectra, the positive cross sections in this region can be attributed to the fact that here stimulated emission occurring on the $^5F_4$,$^5S_2 \rightarrow {}^5I_8$ transition is the dominant effect. In the lower spectra small peaks ranging into the positive region can be seen

#222481 - $15.00 USD Received 4 Sep 2014; revised 10 Nov 2014; accepted 10 Nov 2014; published 10 Dec 2014

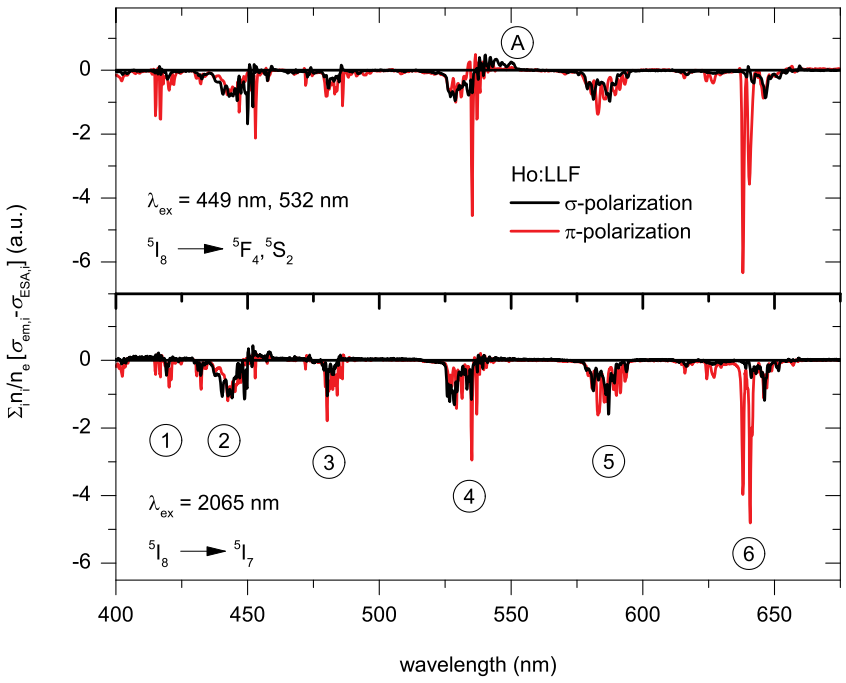

Fig. 6: Polarization dependent ESA spectra of Ho:LLF. The upper part shows spectra recorded with λ_{ex},= 449 nm/532 nm and the lower part with λ_{ex} = 2065 nm. 1 - 6 indicate ESA transitions starting from the $^5I_7$ multiplet while A marks stimulated emission from the $^5F_4$,$^5S_2$ multiplet.

around 450 nm. These, however, can be attributed to an artifact of the measurement since at λ_{ex} = 2065 nm no multiplet is populated which could lead to emission in this spectral region. Taking the results from the derived gain spectra into account it follows that laser operation in the green spectral range with Ho:LLF is in principle possible, provided that the necessary inversion density can be realized. Another point that becomes apparent from the spectra is that ESA occurs for the pump wavelengths around 450 nm and 480 nm. However, ESA processes involving ions populating the trapping multiplet $^5I_7$ and pump photons terminate in multiplets which are coupled to the upper laser level via non-radiative decay channels (cf. Fig. 1). Unfortunately, due to the pronounced ESA bands corresponding to the transitions starting from the multiplet $^5I_7$ it can not be concluded whether or not there is also ESA originating from the upper laser level $^5F_4$,$^5S_2$.

The spectra recorded for Ho:LaF_3 are depicted in Fig. 7. It can be seen that despite the much lower multi-phonon decay rate, ESA bands are present at similar spectral regions as in Ho:LLF. This indicates that in Ho:LaF_3 too, population is trapped in the slow decaying $^5I_7$ multiplet which then acts as starting level for ESA transitions. Nevertheless, around 550 nm the situation is the same as for Ho:LLF, cross sections are positive which means that stimulated emission is dominating. The pump channels are also affected in the same way as in Ho:LLF. In general, due to its much higher quantum efficiency LaF_3 is likely to be a more favorable host matrix for exploiting the green transition in Ho^{3+} than $LiLuF_4$.

#222481 - $15.00 USD Received 4 Sep 2014; revised 10 Nov 2014; accepted 10 Nov 2014; published 10 Dec 2014

Table 4: Multiplets involved in the transitions marked in Fig. 6.

No.	starting multiplet	terminal multiplet
1	$^5I_7$	$^5G_3$, $^3L_9$
2		$^3H_5$, $^3H_6$
3		$^5G_4$, $^5K_7$
4		$^5G_5$
5		$^5G_6$
6		$^5F_3$
A	$^5F_4$,$^5S_2$	$^5I_8$

3. Laser experiments

Laser experiments were carried out in a hemispherical resonator which consisted of a plane input coupling mirror M1 and a curved end mirror M2 (radius of curvature r_{OC} = 50 mm). M1 was anti-reflection coated for the pump wavelength and highly reflective for the wavelength range around 550 nm. Mirrors with different output coupling rates T_{OC} for the laser wavelength were available as M2. The pump beam was focused by a lens through M1 into the gain medium. Lenses with focal lengths of either 30 mm or 50 mm were employed. The crystal was held in a copper heat sink which was water cooled to T = 6°C. As pump sources two different 2ωOPSLs were available, one with λ_{em} = 486.2 nm for Ho:LLF and one with λ_{em} = 479.2 nm for Ho:LaF_3. The maximum output power was in both cases 4 W. However, since 2ωOPSLs exhibited a narrow linewidth ($\Delta\lambda \approx 0.1$ nm) and were not tunable, the pump wavelength could not be optimized. Therefore the spectral overlap between pump and absorption spectrum was rather poor.

Three different samples were employed as gain medium. Two samples were *a*-cut Ho:LLF crystals with lengths of 3.0 mm and 2.3 mm and dopant concentrations of 0.6 at.% and 0.3 at.% respectively. The third sample was a 3 mm long *a*-cut Ho:LaF_3 crystal with a doping concentration of 0.4 at.%.

Independent of the sample, the focal length of the lens, and the output coupling rate of M2 laser operation could not be achieved with Ho:LLF. The reason for this is most likely the strong

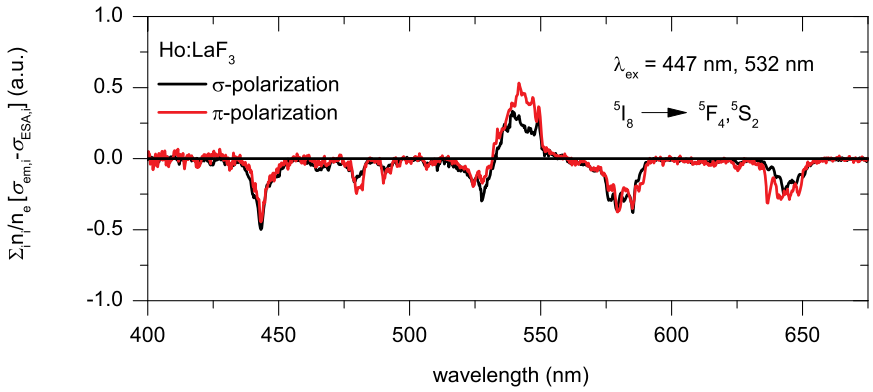

Fig. 7: Polarization dependent ESA spectra of Ho:LaF_3 recorded with λ_{ex},= 447 nm/532 nm.

#222481 - $15.00 USD Received 4 Sep 2014; revised 10 Nov 2014; accepted 10 Nov 2014; published 10 Dec 2014

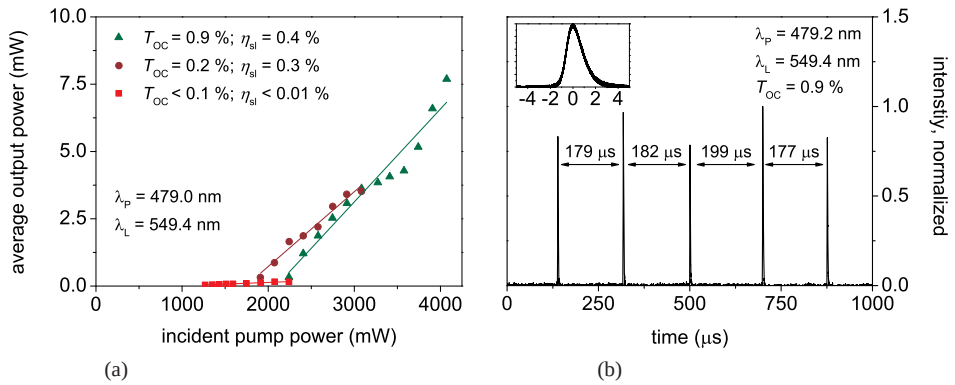

Fig. 8: (a) Input-ouput curves of the 2ωOPSL pumped Ho:LaF_3 laser. (b) Temporal characteristics of a train of pulses at maximum pump power with the inset showing a single pulse.

multi-phonon decay of the upper laser level $^5F_4$,$^5S_2$. This limits the inversion ratio to a value which is not high enough to overcome the reabsorption.

In case of Ho:LaF_3 it was possible to achieve laser operation at a wavelength of $\lambda_L = 549.4$ nm which corresponds to the wavelength predicted by the gain spectra (cf. Fig. 4c/d and Fig. 7). To the best of our knowledge this constitutes the first demonstration of green laser emission at room temperature of a crystalline Ho^{3+}-doped gain medium. The recorded input-output curves for different T_{OC} are depicted in Fig. 8a. Two aspects must be noted. First, due to a non-negligible reflection of the pump light at M2, the quasi-three-level character of the laser, and the linear resonator setup it was not possible to determine exactly how much pump power was absorbed during laser operation. Therefore, in Fig. 8a the incident pump power is given. A simple estimation employing the samples parameters and the Lambert-Beer law yields a single-pass absorption rate of roughly 3 - 4 %. A pump source with a more suitable emission wavelength would thus most likely drastically increase the output power and optical-to-optical efficiency. Second, despite the fact that the gain medium was pumped in a continuous wave regime (cw) all lasers operated in a self-pulsed mode. An exemplary train of pulses and a zoom of a single pulse are depicted in Fig. 8b. The pulse train was recorded with $T_{OC} = 0.9$ % at an incident pump power of $P_{inc} = 4$ W. It can be seen that pulses occur roughly every 180 µs - 200 µs corresponding to a repetition rate of $f_{rep} \approx 5.3$ kHz. The pulse duration was approximately 1.6 µs yielding a peak pulse energy of 1.4 µJ at maximum output power. The reason for the self-pulsing is at the moment unclear. Modeling of the system was so far not possible since the decay dynamics of most of the intermediate Stark multiplets are unknown. Furthermore, the ESA spectra show that it is well possible that even higher multiplets are populated via an ESA transition starting from the upper laser level. Therefore further spectroscopic investigations are necessary to fully understand the dynamics of the system.

It should be noted that experiments were also carried out by in-band pumping Ho:LaF_3 with a frequency doubled Nd^{3+}:YVO_4 laser ($\lambda_{em} = 532$ nm). Laser emission was achieved at $\lambda_L = 549.4$ nm. However, due to a highly unstable operation of the laser which was at least partially the result of a lack of suitable mirrors, a characterization was not possible. Nevertheless this approach seems very interesting due to the extremely small quantum defect of only ≈ 3%.

#222481 - $15.00 USD Received 4 Sep 2014; revised 10 Nov 2014; accepted 10 Nov 2014; published 10 Dec 2014

4. Conclusion

In this publication we investigated the suitability of Ho:LLF and Ho:LaF_3 as gain media for solid state lasers emitting in the visible spectral range.

Ground state absorption spectra were recorded and revealed the presence of two pump channels in the blue spectral region with cross section in the order of 10^{-20} cm^2. Emission and gain spectra were derived from the GSA characteristics and low temperature transmission measurements. Both systems show that gain is possible in the wavelength region around 550 nm if inversion ratios higher than 20 % can be realized. From the decay dynamics of the upper laser level the upper limit of the quantum efficiency of the two materials were estimated to be around 40 % and 75 % for Ho:LLF and Ho:LaF_3 respectively. The necessary inversion density in combination with the quantum efficiency lead to the conclusion that the latter system is most likely better suited as gain medium. Investigations of the ESA revealed for both systems that stimulated emission is the dominant effect at the prospective laser wavelength. However, pronounced ESA was observed starting from the long living multiplet $^5I_7$ which is populated by the strong multi-phononic decay of the upper laser level.

Laser experiments were conducted with both materials. In the case of Ho:LLF it was not possible to achieve laser operation. With Ho:LaF_3 laser emission was demonstrated in the green spectral region at a wavelength of $\lambda_L = 549.4$ nm. To the best of our knowledge this constitutes the the first laser operation of a crystalline Ho^{3+}-doped gain medium in the green spectral region at room temperature. The laser operated in a self-pulsed regime with a maximum slope efficiency with respect to the incident pump power of 0.4 % and a maximum average output power of 7.7 mW. The repetition rate was roughly 5.3 kHz with a pulse duration of 1.6 µs and a peak pulse energy of 1.4 µJ. The reason for the self-pulsing behavior is so far unclear. Further investigations of the decay dynamics of the intermediate and also higher Stark multiplets are necessary to allow for a modeling of the systems which might lead to fully understand the behavior of the laser.

Acknowledgment

The authors gratefully acknowledge the financial support within the framework of the graduate school 1355 “Physics with new advanced coherent radiation sources,” of the Deutsche Forschungsgemeinschaft and the Joachim Herz Stiftung, and the Vigoni project of the Deutscher Akademischer Austauschdienst.

The authors would furthermore like to thank Dr. Philipp Koopmann for his help involving the Tm^{3+}:Lu_2O_3 laser.

#222481 - $15.00 USD Received 4 Sep 2014; revised 10 Nov 2014; accepted 10 Nov 2014; published 10 Dec 2014